HHS Public Access

Author manuscript

J Control Release. Author manuscript; available in PMC 2019 August 10.

Published in final edited form as:

J Control Release. 2018 August 10; 283: 84–93. doi:10.1016/j.jconrel.2018.05.025.

ROS-Triggered Degradable Iron-Chelating Nanogels: Safely Improving Iron Elimination *in Vivo*

Zhi Liu[a], **Jing Qiao**[a], **Tamas Nagy**[b], and **May P. Xiong**[a,*]

[a]Department of Pharmaceutical & Biomedical Sciences, College of Pharmacy, University of Georgia, Athens, GA 30602-2352, USA

[b]Department of Pathology, College of Veterinary Medicine, University of Georgia, Athens, GA 30602-7388, USA

Abstract

Iron-mediated generation of highly toxic Reactive Oxygen Species (ROS) plays a major role in the process leading to iron overload-related diseases. The long-term subcutaneous administration of Deferoxamine (DFO) is currently clinically-approved to improve patient symptoms and survival. However, non-specific toxicity and short circulation times of the drug in humans often leads to poor patient compliance. Herein, thioketal-based ROS-responsive polymeric nanogels containing DFO moieties (rNG-DFO) were designed to chelate iron and to degrade under oxidative stimuli into fragments <10 nm to enhance excretion of iron-bound chelates. Serum ferritin levels and iron concentrations in major organs of IO mice decreased following treatment with rNG-DFO, and fecal elimination of iron-bound chelates increased compared to free DFO. Furthermore, rNG-DFO decreased iron mediated oxidative stress levels *in vitro* and reduced iron-mediated inflammation in the liver of IO mice. The study confirms that ROS-responsive nanogels may serve as a promising alternative to DFO for safer and more efficient iron chelation therapy.

Graphical abstract

ROS-triggered degradable polymeric nanogels post-functionalized with Deferoxamine (rNG-DFO) are prepared to chelate excess iron and improve elimination of iron-bound chelates.

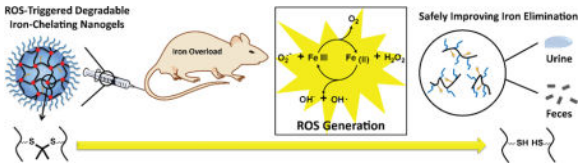

*Corresponding author. mpxiong@uga.edu.

Conflict of Interest

The authors declare no conflict of interest.

Keywords

reactive oxygen species (ROS); nanogel; chelation therapy; iron overload (IO); Deferoxamine (DFO)

1. Introduction

Iron overload (IO), also known as hemochromatosis, is a condition characterized by excessive iron deposition in critical organs of the body, especially liver and heart, which can result in significant structural damage and dysfunction to organs.[1, 2] Surprisingly, although it is one of the most common genetic diseases in the U.S., individuals with the condition typically exhibit few symptoms in the early stages and are often unaware of their condition until it has already progressed to a dangerous level.[3-5] IO can induce cirrhosis of the liver leading to an increased risk of developing liver cancer, contribute to the development of arthritis, and can result in shrinkage of testicles in males leading to impotence.[6-8] Risk factors for IO may also increase even further in patients with diabetes due to selective iron deposition into pancreatic islet β cells which can lead to functional failure of the pancreas.[9] Ultimately, iron accumulation can cause IO-related cardiomyopathies (IOC) such as abnormal heart rhythms or heart failure, and is the primary cause of morbidity and mortality in IO patients.[10, 11] IO is also relevant to neurological diseases and recent studies have demonstrated presence of excess iron in the brains of Alzheimer and Parkinson's disease patients.[12, 13] Due to the obvious prevalence and relevance of IO across such a broad array of diseases, it is imperative to investigate environment-responsive strategies for improving iron chelation therapy based on an understanding of cellular properties unique to the IO condition.

The mainstay approach to alleviate IO is to infuse patients for days with the clinically-approved small molecule metal chelator Deferoxamine (DFO) due to its high binding affinity to ferric iron and rapid elimination from the body.[14, 15] Indeed, a large body of clinical evidence has demonstrated that survival of patients with IO can be significantly increased through the long-term subcutaneous administration of DFO.[16, 17] In spite of the wide-spread use of this drug, critical drawbacks to DFO therapy involve its non-specific toxicity in humans when infused intravenously or intramuscularly and short blood circulation times (half-life of ca. 20 min in humans). [18-20] Clinical evidence has demonstrated that IO conditions can further induce life threatening organ damage and dysfunction such as cardiomyopathies if adequate reduction of iron content is not achieved during DFO therapy. Encouragingly, recent studies have demonstrated that it is possible to overcome existing defects of DFO through the inclusion of the drug into macromolecules. [21-24] Due to the need to efficiently excrete iron-chelates from the body to minimize organ accumulation, environment-responsive systems capable of chelating excess iron and degrading in response to specific triggers unique to IO would be especially attractive but have yet to be thoroughly investigated.

It is well known that excess iron in cells is extremely dangerous to tissues and organs due to iron-mediated generation of highly toxic Reactive Oxygen Species (ROS) via the Haber-

Weiss reaction.[25] This intracellular reaction is believed to be the primary mechanism by which biomolecules such as lipids, proteins, and DNA become damaged.[26] As such, one distinctive feature of IO cells is that they are uniquely under more oxidative stress than non-iron overloaded (NIO) cells and this elevated oxidative stress can therefore serve as a selective trigger for degradation of iron-chelating macromolecules to promote their elimination from the body. In contrast to rapidly cleared free DFO, iron-chelating macromolecules are expected to circulate longer and would have the advantage of being able to more efficiently chelate dangerous non-transferrin bound iron (NTBI)[27] present in the circulation, and be able to naturally target the iron storage pool of the liver.

To investigate this new strategy to improve iron chelation therapy, we have synthesized polymeric nanogels capable of chelating iron and degrading under elevated oxidative stimuli into polymeric fragments <10 nm (28) to promote elimination. In general, nanogels are comprised of a crosslinked polymeric network which can be chemically tailored as desired to improve upon their biocompatible and/or mechanical properties. We have previously demonstrated that nanogels are capable of significantly extending DFO circulation.[29] To prepare these new degradable nanogels, an activated ester–amine crosslinking methodology previously reported by Thayumanavan's group was utilized to generate ROS-responsive nanogels [30] that were then post-functionalized with DFO. Of particular significance is that the ROS-reponsive degradation mechanism of these nanogels results from the incorporation of modified thioketal crosslinkers which have previously been shown to rapidly cleave into ketones and organic thiols (or disulfides) in the presence of ROS.[31-33] As summarized in Scheme 1, final nanogels were generated by crosslinking the amphiphilic random polypentafluorophenyl acrylate polyethylene glycol methacrylate copolymer containing reactive lipophilic pentafluorophenyl groups (PPFPA-*r*-PEGMA) with short thioketal diamine crosslinkers and then following with DFO conjugation to generate ROS-responsive polymeric nanogels containing DFO moieties (rNG-DFO). Owing to its iron chelation capability and degradable properties, rNG-DFO decreased iron burden levels in critical organs and improved total fecal elimination of iron-chelates in an IO mouse model. Studies also demonstrated that rNG-DFO was significantly less cytotoxic to cells *in vitro* and could reduce IO-induced inflammation in the liver of IO rodents compared to free DFO.

2. Materials and methods

2.1. Materials

Unless indicated, all chemicals were used as received from Sigma-Aldrich (St. Louis, MO). Ferric ammonium citrate (FAC) was purchased from VWR (Radnor, PA). Deferoxamine mesylate (DFO) was obtained from the University of Wisconsin Hospital Pharmacy Services (Hospira). Pentafluorophenyl acrylate (PFPA) was synthesized following a reported method. [30] Resazurin, Dulbecco's modified eagle medium (DMEM), heat-inactivated fetal bovine serum (FBS), penicillin/streptomycin solution (100×) and the Pierce BCA protein assay kit were purchased from Thermo Fisher Scientific Inc. Mouse ferritin ELISA kit was purchased from Immunology Consultants Laboratory (Portland, OR). DCFDA cellular ROS detection assay kit was purchased from Abcam (Cambridge, MA). All other reagents were commercially available and used as supplied without further purification. Dextran/Fe

(Anem-X 100) was purchased from Aspen Veterinary Resources, Ltd. Mouse macrophage/monocyte cell line J774A.1 was purchased from American Type Culture Collection (ATCC). Female Balb/C mice, 6 weeks old, were purchased from Taconic Biosciences, USA.

2.2. Synthesis of Material Precursors

See Supporting Information for details.

2.3. Physical Characterizations

All NMR spectra were acquired with a 400 MHz Bruker NMR spectrometer. By scanning between 380–640 nm with a SpectraMax Plus spectrophotometer (Molecular Devices), UV/Vis absorption spectra was used to confirm the iron chelation properties of rNG-DFO (DFO:iron(III) complexes absorb at ca. 430 nm) and quantify the amount of DFO monomers incorporated into the nanogel scaffold. To investigate the morphology of nanogel, transmission electron microscopy (TEM) images were taken on a JEM1011 instrument at an acceleration voltage of 100 kV. Sample was prepared by air-drying a drop of 0.01 mg/mL nanogel suspension on copper grid. Hydrodynamic size and polydispersity (PDI) of rNG-DFO were obtained with a Zetasizer Nano ZS (Malvern Instruments, UK) and analyzed with Zetasizer software v7.10. The cumulant analysis method was used to calculate the z-average diameter and PDI; measurements were conducted on three batches of samples and results are reported as mean ± standard deviation (SD). To study the stability of rNG-DFO under various pH conditions, 1.0 mL nanogel (1 mg/mL) in PBS (pH 7.4), acetate buffer (pH 5.0), or carbonate-bicarbonate buffer (pH 10.0) was incubated at RT; stability of rNG-DFO was analyzed with DLS after 24 and 240 h incubations. To study the degradation behavior of rNG-DFO under oxidative condition as a function of time, individual glass vials containing 1.0 mL nanogels (1 mg/mL) were incubated with 0 or 100 μM H_2O_2 at RT. The vials were sealed with Parafilm to avoid contamination with dust particles, and after 1, 12 and 24 h, samples were removed from each vial for DLS analysis. Molecular weight distribution of the polymers was characterized via gel permeation chromatography (GPC) using 0.1% (v/v) LiBr/DMF solution as eluent at a flow rate of 1.0 mL/min and calibrated with respect to polystyrene standards. GPC data was analyzed with Shimadzu LCsolution GPC postrun software. IR spectra were obtained on a Nicolet 380 FTIR. Mass spectrometry data was acquired by the University of Georgia Proteomics and Mass Spectrometry Core Facility on a Bruker Esquire 3000 Plus Ion Trap Spectrophotometer and a Bruker Autoflex (TOF) mass spectrometer.

2.4. Cytotoxicity Studies

The *in vitro* cytotoxicity of rNG-DFO was investigated in J774A.1 macrophage cells through a metabolism-based resazurin assay. Cells were seeded in 96-well plates at a density of 10,000 cells/well, incubated at 37°C, 5% CO_2 and 100% humidity with DMEM complete medium containing 10% FBS and 1% penicillin/streptomycin for 24 h. Cells were then treated with DFO, rNG-DFO, or equivalent degraded fragments of rNG-DFO at comparable final DFO concentrations up to 1 mM prepared by 1:3 serial dilutions. In addition, the cytotoxicity of control nanogels not conjugated to DFO (rNG) and its corresponding degraded fragments, and acetone (a relevant degradation product of thioketal cleavage) were also investigated. After 48 h incubation with the various treatments, 100 μL of resazurin (44

μM) in cell culture medium was added to each well and incubated at 37°C for 4 h. The fluorescence was measured by exciting at 560 nm and measuring emission at 590 nm on a SpectraMax Gemini EM microplate reader. Readings from wells without cells were used as E_{blank}, and the readings from control cells without treatment ($E_{control}$) represented 100% cell viability. The viability of cells can be calculated by the following equation:

$$Cell\ vaibillity = 100 \times \frac{E_{sample} - E_{blank}}{E_{control} - E_{blank}}\%$$

Similarly, cytotoxicity was also evaluated in J774A.1 cells that had been iron overloaded prior to treatment. IO was induced in cells by incubation with culture medium containing 100 μM ferric ammonium citrate (FAC) for 24 h (cells >80% viable with FAC incubation, data not shown) prior to the cytotoxicity study with the various treatments.

2.5. *In Vitro* Ferritin Reduction Assay

J774A.1 macrophage cells were seeded in 6-well plates at a density of 30,000 cell/well and allowed to settle for 24 h at 37°C, 5% CO_2 and 100% humidity with DMEM complete medium before treatment. The cells were treated with culture medium containing 100 μM FAC for 24 h to induce IO as described above. Subsequently, cells were washed with PBS and treated with DFO or rNG-DFO at 10 and 50 μM. Equivalent rNG based on w/v to rNG-DFO concentrations was also investigated. After 48 h incubation, cells were lysed with cell lysis buffer (150 mM NaCl, 10 mM Tris, 1% Triton X-100 and protease inhibitor cocktail, pH 7.4). Total protein concentration was measured with the BCA protein assay kit and cellular ferritin concentration was measured with a mouse ferritin ELISA kit. The results are plotted as the ratio of ng of ferritin per μg total protein concentration.

2.6. Measuring Iron-Mediated Oxidation Stress Levels in the Presence of Iron Chelators

The DCFDA cellular ROS detection assay kit was used to determine the capability of rNG-DFO to reduce iron-mediated oxidative stress in IO cells. Briefly, J774A.1 macrophage cells were seeded in 96-well plates at a density of 10,000 cells/well incubated at 37°C, 5% CO_2 and 100% humidity with DMEM complete medium for 24 h prior to treating with culture medium containing 100 μM FAC for 24 h to induce IO. Subsequently, cells were washed with PBS and treated with either 50 μM DFO or equivalent rNG-DFO for 8 h; equivalent rNG based on w/v to rNG-DFO concentrations was also investigated as a control. Next, non-fluorescent DCFDA solution was added to each well at a final concentration of 20 μM for 30 min at 37°C. Cells were washed, and H_2O_2 was added to each well at a final concentration of 50 μM; the fluorescence change was measured at indicated times using a SpectraMax Gemini EM microplate reader by exciting at 485 nm and measuring emission at 535 nm at 37°C. NIO cells that had not been treated with chelators but had been treated with DCFDA served as control blanks.

2.7. *In Vivo* Elimination Studies

All animal experiments were conducted in accordance with the University of Georgia Animal Care and Use Committee guidelines and the NIH Guide for the Care and Use of

Laboratory Animals. Female Balb/C mice, 6 weeks old, were housed in cages in a room maintained at 20 ± 1 °C and with 12 h light and dark cycles. Feed (Harlan Teklad 8604 Rodent Diet) and water were available *ad libitum*. Mice were IO by a single tail vein injection of Dextran/Fe (Anem-X 100, Aspen Veterinary Resources, Ltd; 150 mg/kg of Fe, 10 μl/g BW in normal saline) on Day 1. On Day 8, three mice were randomly housed into each metabolic chamber and started on iron-deficient powder diet (Teklad TD.80396.PWD) *ad libitum*. The following 4 treatments were administered intravenously to animals on Day 8 and every other day for a total of 5 doses: Group 1 = NIO control mice received saline; Group 2 = IO mice received saline; Group 3 = IO mice received DFO at 150 mg/kg; Group 4 = IO mice received rNG-DFO at an equivalent concentration of 150 mg/kg DFO. Mice were monitored daily and bw were recorded on alternate days, and necropsied 7 days following administration of the last treatment dose. To quantify elimination of iron from animals, feces and urine were collected daily from metabolic chambers and weighed throughout the duration of the study. Fecal material was homogenized in distilled water, iron was extracted from the homogenate by the addition of 5% Trichloroacetic acid (TCA)/1.5 N HCl, and the extract was heated to 70°C for 90 mins. Final iron concentration in urine and feces was measured by standard atomic absorption spectroscopy (AAS; GBC Scientific Equipment model 932AA). Mice were euthanized by CO_2 overdose and blood was directly collected via cardiac puncture and added to microcentrifuge tubes to separate out the serum for ferritin measurements by ELISA assay based on the manufacturer's instructions. The lungs, heart, spleen, kidneys, brain and liver of animals were subsequently harvested, rinsed with fresh PBS, blotted dry with Whatman filter paper, and then weighed (note that organ weight is reported as mg of total organ weight per g of animal bw, mg/g). Next, organs were sectioned into different portions and snap-frozen in liquid nitrogen or fixed in neutral buffered formalin. To measure iron content in organs, portions of the snap-frozen tissues were homogenized as described for feces and diluted as needed prior to AAS.

2.8. Histopathological Studies

The histopathological studies were done by blinded evaluation. For histopathological evaluations, portions of organ samples fixed in neutral buffered formalin were embedded in paraffin, sectioned into 5 μm slices, and stained with H&E. A board certified pathologist took photomicrographs, analyzed tissues for abnormalities, and scored all images without prior knowledge of the different treatment groups.

2.9 Statistical Analysis

Statistical analysis was performed with GraphPad Prism 5.0 software. Statistical significance between groups was assessed with one way ANOVA; $p<0.05$ was considered statistically significant.

3. Results and discussion

3.1. Preparation and Physical Characterizations

PPFPA-*r*-PEGMA and ROS-cleavable thioketal crosslinkers containing amino groups were synthesized (Fig. S1 and S2) and their structures were confirmed by ^{1}H NMR spectroscopy (Fig. S3 and S4). A facile surfactant-free method [30] was utilized to prepare rNG-DFO by

mixing polymers containing activated esters (PPFPA-*r*-PEGMA) and short thioketal diamine crosslinkers in a solution of THF and allowing for random crosslinking to generate ROS-responsive nanogels, which were then post-functionalized with DFO moieties (Scheme 1); control nanogels without DFO were also similarly fabricated (rNG). The crosslinking reaction was monitored by FTIR. As shown in Fig. S5A, the peak at 1640 cm^{-1} corresponding to stretching of the amide carbonyl group appeared and the peak at 1780 cm^{-1} ascribed to stretching of the activated ester carbonyl group in pentafluorophenyl (PFP) moieties disappeared partially (not completely since not all activated esters of PFP reacted during the crosslinking reaction). After adding DFO to the reaction to functionalize resulting nanogels, the activated ester C═O signal of remaining PFP disappeared, confirming conversion of the ester to the amide due to successful DFO conjugation. To further confirm the crosslinking reaction occurred, the process was also monitored by ^{19}F NMR (Fig. S5B). The initial polymer PPFPA-*r*-PEGMA shows three broad peaks at −152.1, −157.1, and −162.0 ppm in the ^{19}F NMR spectrum. After adding thioketal diamine crosslinkers to the reaction, new signals located at −164.6, −167.2 and −176.9 ppm corresponding to the PFP leaving group appeared, along with peaks corresponding to remaining unreacted PFP. These remaining unreacted PFP peaks were broader and completely disappeared after the addition of DFO to the reaction, thus confirming successful post-functionalization of DFO to the crosslinked nanogel.

The morphological structure of rNG-DFO was examined by transmission electron microscopy (TEM), with representative TEM micrographs revealing near-spherical shapes with diameters of ca. 150 nm as shown in Fig. 1A. The apparent size of nanogels was measured by dynamic light scattering (DLS). As shown in Fig. 1B, DLS displayed a single peak characterized by a z-average diameter of ca. 240 nm and a polydispersity index (PDI) of 0.17. The difference in size between TEM and DLS may be attributed to nanogel shrinkage during the preparative process of air-drying TEM samples.[22] To further verify that rNG-DFO are indeed stable crosslinked networks of polymers rather than an aggregation of the polymers, final rNG-DFO were re-dispersed in THF and characterized by DLS in THF; their z-average diameter remained near ca. 240 nm similar to the size reported in H_2O (Fig. S6A). Specifically, prior to the crosslinking reaction, the apparent size of the initial polymer PPFPA-*r*-PEGMA in THF or H_2O was <10 nm at the same concentration; after the crosslinking reaction, resulting nanogels formed were much larger in size than the un-crosslinked polymers, whether in THF or H_2O, and these results further support the successful formation of a nanosized covalently crosslinked network.

3.2. Degradation Studies

Oxidative stress levels are typically much higher in IO patients[26] due to the generation of ROS via the Haber-Weiss reaction.[34]. Thioketals are known to be quite stable under acidic and basic conditions but can be rapidly cleaved under oxidative stimuli.[31] To investigate whether rNG-DFO can indeed degrade under oxidative stimuli, nanogels were incubated with 100 μM H_2O_2 and monitored by DLS. H_2O_2 is a natural product of cellular respiration and has been previously used to generate oxidative stress in IO cells.[22] As shown in Fig. 1B, the size of nanogels effectively decreased from ca. 240 nm to ca. <10 nm after 24 h of incubation in an oxidative environment, with the smaller degradation fragments being

critical for facilitating clearance of iron-bound polymer chelates from the body. In contrast, rNG-DFO incubated at pH 5, 7.4, and 10 were quite stable and no size changes in the nanogels were observed after 24 or 240 h incubations (Fig. S6B). In addition, the dispersion of rNG-DFO visually appeared slightly bluish in color, similar to an emulsion solution, and became clear in color after degradation of nanogels in the oxidative environment.

The degradation of rNG-DFO *in vitro* was further monitored by ^{1}H NMR spectroscopy. As the nanogel degrades due to thioketal cleavage, a relevant degradation product of the reaction, acetone, should be generated. Although the peak corresponding to the thioketal linkage in the nanogel at about 1.60 ppm overlaps with the peak corresponding to the polymer backbone, ^{1}H NMR spectrum clearly confirms the generation of acetone at $\delta = 2.10$ ppm (Fig. S7), which is in agreement with a previous study [35]. The change in molecular weight of degraded polymer fragments after cleavage compared to the initial polymers (PPFPA-*r*-PEGMA) was further investigated by GPC and MALDI-MS (Fig. S8). During the nanogel preparation process, the polymer backbone was conjugated to lower molecular weight crosslinkers, releasing the higher molecular weight PFP moieties from the backbone. Thus, after the scission of the crosslinkers under oxidative stimuli, the molecular weight of the degraded polymer fragments should be ca. 3K less than the initial polymers. As shown in Fig. S8, the molecular weight of the polymers decreased from $Mn_{(MALDI)} = 9106$ and $Mn_{(GPC)} = 9457$ to $Mn_{(MALDI)} = 6849$ and $Mn_{(GPC)} = 6759$, which is consistent with our theoretical calculations. These studies suggest that particle degradation is indeed due to scission of the crosslinker rather than due to polymer chain scission. Together, these results indicate that the thioketal linkages were efficiently cleaved by ROS, resulting in the complete dissolution of nanogels into fragments <10 nm for more efficient elimination of macromolecules.[28]

3.3. Iron Chelating Properties

Iron chelating properties of rNG-DFO were confirmed by UV-Vis spectroscopy. The magnitude of the absorbance peak at 430 nm characteristic of the DFO:iron(III) complex was used to generate an equation relating DFO concentration to absorption as previously reported.[21, 22] Only free DFO and rNG-DFO displayed typical absorptions at 430 nm in the presence of iron(III)[36] (Fig. 1C). After washing free DFO:iron(III) and rNG-DFO:iron(III) solutions extensively with a centrifugal filtration unit with a molecular weight cutoff (MWCO) of 10 kDa, the absorption peak at 430 nm was only observable in the recovered orange concentrate of rNG-DFO:iron(III) but not in its filtrate; in contrast, absorptions at 430 nm were present in both the concentrate and filtrate of DFO:iron(III) (Fig. S9). This study further confirms that DFO was successfully conjugated to the nanogel scaffold and not just loosely associated with it. Moreover, because of the linear relationship that exists between absorbance and the concentration of DFO:iron(III) complexes in solution,[37] the absorption intensity at 430 nm can also be used to measure the content of DFO present in the nanomaterial. Based on a methodology we have previously described, [21, 22, 24] the mass fraction of DFO present in rNG-DFO (w/w) was found to be 7.23 %.

3.4. *In Vitro* Cytotoxicity and Ferritin Reduction Assays

The metabolism-based resazurin assay was used to investigate cell viability of rNG-DFO compared to equivalent free amounts of DFO at a concentration ranging from 0.05-1000 μM in J774A.1 mouse macrophage cells (Fig. 2A). The result shows that DFO inhibited 50% cell viability at ca. 13 μM whereas rNG-DFO inhibited 50% cell viability at ca. 700 μM in NIO cells; similar data were obtained in IO cells where free DFO inhibited 50% cell viability at ca. 15 μM compared to rNG-DFO at 900 μM equivalent DFO concentrations. The degraded polymer fragments of rNG-DFO exhibited a similar toxicity profile to rNG-DFO as shown in Fig. S10A (50% cell viability at ca. 750 μM in NIO cells and at ca. 1000 μM in IO cells), and the nanogel backbone overall appeared non-toxic to cells. Acetone, which would have been generated during the degradation of rNG-DFO, did not show cytotoxicity at concentrations as high as 1.2 mg/mL (Fig. S10B). These cytotoxicity studies revealed that the nanogel formulations were overall less toxic to cells compared to the free drug.

A mouse ferritin ELISA kit was used to investigate the ferritin reduction efficacy in IO cells. As previously described, J774A.1 cells were incubated with 100 μM FAC for 24 h, which leads to increased cellular ferritin expression levels from a baseline of 5.51 ng/μg total protein to 9.82 ng/μg ($p < 0.001$) (Fig. 2B). After treating for 48 h with 10 or 50 μM free DFO, cellular ferritin levels reduced to 5.48 ng/μg total protein (44.2% decrease, $p < 0.001$) for 10 μM and even further to 2.90 ng/μg total protein (70.4% decrease, $p < 0.001$) for 50 μM. At the equivalent rNG-DFO concentration, ferritin levels decreased to 5.00 ng/μg total protein (49.1% decrease, $p < 0.001$) when administered at 10 μM and decreased to 3.10 ng/μg total protein (68.4% decrease, $p < 0.001$) at 50 μM. Free DFO and rNG-DFO had similar treatment effects (*ns*) at both concentrations investigated. As a control, rNG was not able to affect ferritin levels in cells, which confirms that DFO was indeed responsible for the iron chelation effect. Ferritin concentrations for both DFO and rNG-DFO formulations were significantly decreased compared to the normal baseline level when treated at 50 μM and could be indicative of too much iron being chelated, which may explain the apparent cytotoxicity of rNG-DFO at higher concentrations.[24] Optimized dosing to prevent chelating too much iron will be an important parameter to consider in future in order to minimize undesirable side effects, but overall results do demonstrate that rNG-DFO is as effective and a much safer choice, in terms of cytotoxicity, for chelating excess iron compared to free DFO.

3.5. Measuring Iron-Mediated Oxidation Stress Levels in the Presence of Iron Chelators

IO is closely associated with increased levels of oxidative stress in the body due to the generation of highly toxic ROS via the Haber-Weiss reaction. To investigate whether rNG-DFO can reduce the effect of iron-mediated oxidative stress in cells, the DCFDA cellular ROS detection assay kit was used since DCFDA is a ROS-sensitive fluorescent dye that can measure a wide variety of ROS produced within the cell.[38, 39] Briefly, J774A.1 macrophage cells were IO by incubating with 100 μM FAC as previously described and then treated with either 50 μM DFO or equivalent rNG-DFO. Next, a solution of DCFDA at 20 μM final concentration was added to each well prior to the addition of 100 μL of 50 μM H_2O_2. The fluorescence change for each treatment group was measured at the indicated

times by exciting at 485 nm and measuring the emission at 535 nm at 37°C. NIO cells without treatments but with DCFDA added were used as blank controls. Iron chelators are expected to reduce oxidative stress levels in cells by chelating iron and thus blocking iron's catalytic properties therefore the fluorescence intensity in IO cells should be significantly higher compared to controls or to IO cells treated with rNG-DFO or DFO during the incubation period (Fig. 2C). There was no significant change in the fluorescence intensity after rNG treatment due to its inability to chelate iron and thus prevent ROS generation. The results confirm that ROS generation levels in IO cells can be effectively reduced through the addition of iron chelators such as rNG–DFO or free DFO.

3.6. *In Vivo* Elimination Studies

The efficiency of iron binding and exclusion was investigated *in vivo* in an IO mouse model, as previously reported.[21] Normal female Balb/C mice (6 weeks old) were iron overloaded by a single tail vein injection of 150 mg/kg Fe/dextran (Day 1). After a week of monitoring animals to ensure adequate ferritin levels indicative of IO, treatment with either 150 mg/kg free DFO or equivalent rNG-DFO was started on Day 8. A total of 5 doses for each treatment group were administered every other day, and all mice were sacrificed on Day 22.

Ferritin is an important protein found throughout cells in the body and is involved in the storage of iron as well as its homeostatic regulation. Serum ferritin concentration is commonly used in clinical settings to screen for IO. High levels of serum ferritin are typically reflective of systemic IO and serves as an easily measurable parameter to quantify the severity of IO.[40, 41] As expected, serum ferritin levels were much higher in untreated IO mice compared to NIO mice ($p < 0.0001$). IO mice treated with DFO reveal that the free drug could not effectively reduce serum ferritin levels compared to untreated IO mice (*ns*), most likely due to its well-known short circulation time and fast clearance in the mouse, and only those IO mice treated with rNG-DFO displayed significantly reduced serum ferritin levels compared to untreated IO mice ($p < 0.001$) or compared to those treated with DFO ($p < 0.001$) (Fig. 3A). We have previously confirmed that nanogel-DFO macromolecules can significantly extend the circulation time of DFO,[29] therefore the decrease in serum ferritin levels may be a result of the prolonged circulation of rNG-DFO compared to free DFO. The urine and feces for the different treatment groups were collected using metabolic cages throughout the duration of the study and the total iron content present was measured by standard atomic absorption spectroscopy (AAS) to compare the iron exclusion levels for each treatment group. As shown in Fig. 3B, significant iron exclusion through the urine was observed for both DFO and rNG–DFO compared to NIO mice and untreated IO mice ($p < 0.001$ and $p < 0.0001$, respectively). Moreover, urine iron content was similar between DFO and rNG-DFO groups at similar doses (*ns*). Total iron exclusion through the feces is shown in Fig. 3C and reveals that a significant increase in iron excretion was observed for both treatment groups (DFO and rNG–DFO) compared to NIO mice and untreated IO mice ($p < 0.01$ and $p < 0.0001$, respectively), however rNG–DFO was significantly superior at promoting iron excretion through feces compared to DFO ($p < 0.001$). The improved iron excretion results observed for rNG-DFO may be explained by the greater levels of oxidative stress present in cells of IO mice, which is expected to significantly enhance thioketal cleavage for faster breakdown of the nanogel and promote elimination of iron-bound

chelates. The increased exclusion of iron via the liver through feces is likely due to the localization of larger macromolecular iron chelators such as rNG-DFO to the liver, which may be advantageous since the vast majority of ferritin for storing iron is present in Kupffer cells and hepatocytes of this major organ.

To further probe the iron elimination capability of rNG-DFO compared to DFO, organs (heart, liver, spleen, and kidney) from sacrificed mice were homogenized and iron content in each tissue was measured by AAS (Fig. 4). AAS data indicates overall that there was a downward trend in iron content for liver, spleen, heart and kidneys of mice treated with both DFO and rNG-DFO compared to untreated IO mice ($p < 0.05$ for all comparisons). However, rNG–DFO was superior at mobilizing iron away from the liver, heart, and kidneys compared to free DFO at equivalent doses ($p < 0.05$ for all comparisons), with the exception of spleen where there was no significant difference between the two treatment groups (*ns*) due to the natural abundance of iron in this organ. Moreover, there were significant differences in iron concentrations in the heart of rNG-DFO vs. untreated IO mice ($p < 0.01$) and rNG-DFO vs. DFO-treated mice ($p < 0.01$), indicating that rNG-DFO chelated NTBI more effectively away from the heart compared to free DFO in spite of similar dosing regimens. This finding is extremely encouraging since NTBI accumulation into heart tissues can ultimately be fatal in patients. It should be noted that even after 5 treatments of DFO or rNG-DFO to IO mice, AAS data revealed that the iron concentration level in all the organs was still overall higher than that of NIO mice, and optimization of our IO animal model as well as the structural features of nanomaterials to further enhance iron binding properties and elimination *in vivo* are in progress. Overall, these elimination data coupled with the decreased serum ferritin measurements suggest considerably more efficient mobilization of iron away from major organs of rodents treated with rNG-DFO compared to free DFO.

3.7. Acute Toxicity Studies

To assess the acute toxicity properties of the chelators, the body weights (BW) of mice were measured during the entire course of treatment. BW of mice receiving rNG-DFO and DFO treatments did not decrease and remained within the normal range of ±15% BW compared to NIO and untreated IO mice (Fig. 5A). Organ weights (lungs, heart, spleen, kidneys, brain, and liver) were also measured after animals were sacrificed and compared to NIO and untreated IO mice; overall, the weight of clearance organs such as the spleen and liver of animals receiving DFO and rNG-DFO remained within the normal range of ±15% compared to NIO and untreated IO mice (*ns*) (Fig. 5B). This indicates that rNG-DFO did not induce acute toxicities in animals even after 5 doses, which would typically be characterized by enlargements of the spleen and liver, and could be a result of the nanomaterial's ROS-induced degradable properties.

The safety of rNG-DFO in mice was also confirmed with histopathology by analyzing tissue samples of major organs sectioned and stained with hematoxylin and eosin (H&E). Final images taken were blindly examined and scored by a board certified pathologist. As summarized in Table 1, no abnormality or lesions (inflammation around hemosiderin-laden cells) were observed in the histological appearance of spleen, heart, kidney, lung and brain of IO mice. There were however many more multifocal inflammatory foci around

hemosiderin-laden cells in the livers of untreated IO mice, which could be a side effect of excessive iron deposition. Interestingly, only rNG-DFO treatment was noted to relieve such inflammation in the livers of IO-treated mice, which was significant enough to merit a score of (+) for rNG-DFO compared to untreated IO and DFO-treated groups (both ++).

Representative images of some of these hepatic inflammatory foci noted in the liver are shown in Fig. 6. In general, at low magnification, scattered small foci of hypercellularity and scattered iron-containing cells could be seen more predominently in both untreated IO and DFO-treated groups, whereas fewer foci of hypercellularity were observed after rNG-DFO treatment. Moreover, at higher magnification, the photomicrograph suggests less evidence of inflammation following rNG-DFO treatments due to minute presence of inflammatory cells around hemosiderin-laden Kupffer cells and minimal cellular debris compared to untreated IO and DFO-treated groups. This is perhaps the result of more effective iron chelation by rNG-DFO compared to DFO, as evidenced by the decreased iron-mediated inflammation in the liver, and likely also arising perhaps from the improved clearance of nanogels due to the ROS-dependent degradation mechanism that was incorporated into the design.

4. Conclusion

In summary, a facile method was utilized to generate thioketal-crosslinked polymeric nanogels post-functionalized with DFO moieties to chelate iron (e.g. rNG-DFO). rNG-DFO was shown to degrade under oxidative conditions into fragments <10 nm for improved elimination. In addition, rNG-DFO did not induce cytotoxicity in cells nor display signs of acute toxicity in mice at therapeutic doses administered. Furthermore, rNG-DFO decreased iron-mediated oxidative stress levels *in vitro* and reduced evidence of IO-related inflammation in the liver of mice. Moreover, rNG-DFO exhibited excellent iron binding and exclusion capabilities as evidenced by decreased serum ferritin levels and improved total fecal elimination of iron-bound chelates. Overall, ROS-triggered degradable nanogels have shown potential for safely improving iron elimination *in vivo*.

Supplementary Material

Refer to Web version on PubMed Central for supplementary material.

Acknowledgments

This work was supported by NIH grant R01DK099596 awarded to M.P. Xiong.

Appendix A. Supplementary data

Supplementary data to this article can be found online

References

1. Andrews NC. Iron metabolism: iron deficiency and iron overload. Annu Rev Genomics Hum Genet. 2000; 1:75–98. [PubMed: 11701625]
2. Siddique A, Kowdley KV. Review article: the iron overload syndromes. Aliment Pharmacol Ther. 2012; 35:876–893. [PubMed: 22385471]

3. Weatherall DJ. The inherited diseases of hemoglobin are an emerging global health burden. Blood. 2010; 115:4331–4336. [PubMed: 20233970]
4. Modell B, Darlison M. Global epidemiology of haemoglobin disorders and derived service indicators. Bull W H O. 2008; 86:480–487. [PubMed: 18568278]
5. Weatherall DJ, Clegg JB. Thalassemia–a global public health problem. Nat Med. 1996; 2:847–849. [PubMed: 8705845]
6. Niederau C, Fischer R, Sonnenberg A, Stremmel W, Trampisch HJ, Strohmeyer G. Survival and causes of death in cirrhotic and in noncirrhotic patients with primary hemochromatosis. N Engl J Med. 1985; 313:1256–1262. [PubMed: 4058506]
7. Adams PC, Deugnier Y, Moirand R, Brissot P. The relationship between iron overload, clinical symptoms, and age in 410 patients with genetic hemochromatosis. Hepatology. 1997; 25:162–166. [PubMed: 8985284]
8. Allen KJ, Gurrin LC, Constantine CC, Osborne NJ, Delatycki MB, Nicoll AJ, McLaren CE, Bahlo M, Nisselle AE, Vulpe CD, Anderson GJ, Southey MC, Giles GG, English DR, Hopper JL, Olynyk JK, Powell LW, Gertig DM. Iron-overload-related disease in HFE hereditary hemochromatosis. N Engl J Med. 2008; 358:221–230. [PubMed: 18199861]
9. Lu JP, Hayashi K. Selective iron deposition in pancreatic islet B cells of transfusional iron-overloaded autopsy cases. Pathol Int. 1994; 44:194–199. [PubMed: 8025661]
10. Gujja P, Rosing DR, Tripodi DJ, Shizukuda Y. Iron overload cardiomyopathy: better understanding of an increasing disorder. J Am Coll Cardiol. 2010; 56:1001–1012. [PubMed: 20846597]
11. Kremastinos DT, Farmakis D. Iron overload cardiomyopathy in clinical practice. Circulation. 2011; 124:2253–2263. [PubMed: 22083147]
12. Zecca L, Youdim MBH, Riederer P, Connor JR, Crichton RR. Iron, brain ageing and neurodegenerative disorders. Nat Rev Neurosci. 2004; 5:863–873. [PubMed: 15496864]
13. Barnham KJ, Bush AI. Metals in Alzheimer's and Parkinson's diseases. Curr Opin Chem Biol. 2008; 12:222–228. [PubMed: 18342639]
14. Heli H, Mirtorabi S, Karimian K. Advances in iron chelation: an update. Expert Opin Ther Pat. 2011; 21:819–856. [PubMed: 21449664]
15. Hoffbrand AV, Taher A, Cappellini MD. How I treat transfusional iron overload. Blood. 2012; 120:3657–3669. [PubMed: 22919029]
16. Propper RD, Cooper B, Rufo RR, Nienhuis AW, Anderson WF, Bunn HF, Rosenthal A, Nathan DG. Continuous subcutaenous administration of deferoxamine in patients with iron overload. N Engl J Med. 1977; 297:418–423. [PubMed: 882111]
17. Brittenham GM. Iron-chelating therapy for transfusional iron overload. N Engl J Med. 2011; 364:146–156. [PubMed: 21226580]
18. Porter JB, Faherty A, Stallibrass L, Brookman L, Hassan I, Howes C. A trial to investigate the relationship between DFO pharmacokinetics and metabolism and DFO-related toxicity. Ann N Y Acad Sci. 1998; 850:483–487. [PubMed: 9668591]
19. Levine JE, Cohen A, MacQueen M, Martin M, Giardina PJ. Sensorimotor neurotoxicity associated with high-dose deferoxamine treatment. J Pediatr Hematol/Oncol. 1997; 19:139–141.
20. Olivieri NF, Buncic JR, Chew E, Gallant T, Harrison RV, Keenan N, Logan W, Mitchell D, Ricci G, Skarf B, Taylor M, Freedman MH. Visual and auditory neurotoxicity in patients receiving subcutaneous deferoxamine infusions. N Engl J Med. 1986; 314:869–873. [PubMed: 3485251]
21. Liu Z, Lin TM, Purro M, Xiong MP. Enzymatically biodegradable polyrotaxane-deferoxamine conjugates for iron chelation. ACS Appl Mater Interfaces. 2016; 8:25788–25797. [PubMed: 27623539]
22. Liu Z, Wang Y, Purro M, Xiong MP. Oxidation-induced degradable nanogels for iron chelation. Sci Rep. 2016; 6:20923. [PubMed: 26868174]
23. ul-haq MI, Hamilton JL, Lai BFL, Shenoi RA, Horte S, Constantinescu I, Leitch HA, Kizhakkedathu JN. Design of long circulating nontoxic dendritic polymers for the removal of iron in vivo. Acs Nano. 2013; 7:10704–10716. [PubMed: 24256569]
24. Liu Z, Purro M, Qiao J, Xiong MP. Multifunctional polymeric micelles for combining chelation and detection of iron in living cells. Adv Healthcare Mater. 2017; 6:170016.

25. Kehrer JP. The Haber-Weiss reaction and mechanisms of toxicity. Toxicology. 2000; 149:43. [PubMed: 10963860]
26. Dixon SJ, Stockwell BR. The role of iron and reactive oxygen species in cell death. Nat Chem Biol. 2014; 10:9–17. [PubMed: 24346035]
27. Brissot P, Ropert M, Le Lan C, Loreal O. Non-transferrin bound iron: a key role in iron overload and iron toxicity. Biochim Biophys Acta, Gen Subj. 2012; 1820:403–410.
28. Tang SH, Chen M, Zheng NF. Sub-10-nm Pd nanosheets with renal clearance for efficient near-infrared photothermal cancer therapy. Small. 2014; 10:3139–3144. [PubMed: 24729448]
29. Wang Y, Liu Z, Lin TM, Chanana S, Xiong MP. Nanogel-DFO conjugates as a model to investigate pharmacokinetics, biodistribution, and iron chelation in vivo. Int J Pharm. 2018; 538:79–86. [PubMed: 29341909]
30. Zhuang JM, Jiwpanich S, Deepak VD, Thayumanavan S. Facile preparation of nanogels using activated ester containing polymers. Acs Macro Lett. 2012; 1:175–179.
31. Xu QH, He CL, Xiao CS, Chen XS. Reactive oxygen species (ROS) responsive polymers for biomedical applications. Macromol Biosci. 2016; 16:635–646. [PubMed: 26891447]
32. Lee SH, Gupta MK, Bang JB, Bae H, Sung HJ. Current progress in reactive oxygen species (ROS) responsive materials for biomedical applications. Adv Healthcare Mater. 2013; 2:908–915.
33. Saravanakumar G, Kim J, Kim WJ. Reactive oxygen species responsive drug delivery systems: promises and challenges. Adv Sci. 2017; 4:1600124.
34. Burkitt MJ, Mason RP. Direct evidence for in vivo hydroxyl-radical generation in experimental iron overload: an ESR spin-trapping investigation. Proc Natl Acad Sci USA. 1991; 88:8440–8444. [PubMed: 1656444]
35. Shim MS, Xia YN. A reactive oxygen species (ROS)-responsive polymer for safe, efficient, and targeted gene delivery in cancer cells. Angew Chem, Int Ed. 2012; 52:6926–6929.
36. Goodwin JF, Whitten CF. Chelation of ferrous sulphate solutions by desferrioxamine B. Nature. 1965; 205:281–283. [PubMed: 14270711]
37. Keberle H. Ann. The biochemistry of desferrioxamine and its relation to iron metabolism. N Y Acad Sci. 1964; 119:758–768.
38. Wu DL, Yotnda P. Production and detection of reactive oxygen species (ROS) in cancers. J Visualized Exp. 2011; 57:1.
39. Kalyanaraman B, Darley-Usmar V, Davies KJA, Dennery PA, Forman HJ, Grisham MB, Mann GE, Moore K, Roberts LJ, Ischiropoulos H. Measuring reactive oxygen and nitrogen species with fluorescent probes: challenges and limitations. Free Radical Biol Med. 2012; 52:1–6. [PubMed: 22027063]
40. Lipschitz DA, Cook JD, Finch CA. A clinical evaluation of serum ferritin as an index of iron stores. N Engl J Med. 1974; 290:1213–1216. [PubMed: 4825851]
41. Cook JD, Lipschit DA, Miles LEM, Finch CA. Serum ferritin as a measure of iron stores in normal subjects. Am J Clin Nutr. 1974; 27:681–687. [PubMed: 4472911]

Highlights

- Degradable nanogels (rNG-DFO) are prepared for iron chelation
- No sign of acute toxicity at 150 mg/kg/dose equivalent DFO (5 doses)
- There was less iron-overload related inflammation in the liver
- Mice treated with rNG-DFO had decreased serum ferritin
- Total fecal elimination of iron-bound chelates increased

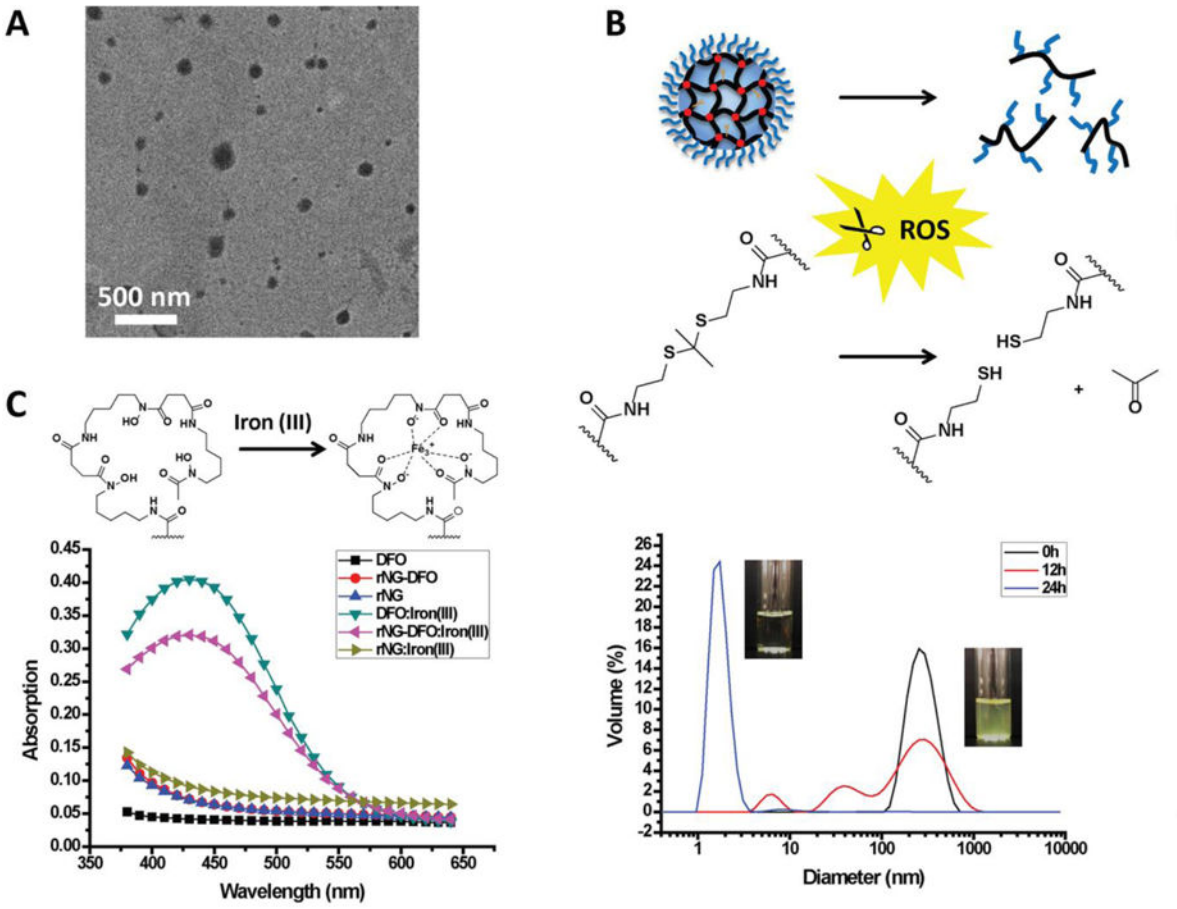

Fig. 1.

(A) Representative TEM image of rNG-DFO (scale: 500 nm). **(B)** Under oxidative stimuli, thioketals in the nanogels cleave and acetone is released as nanogels degrade into water-soluble polymeric fragments. Shown below are degradation profiles as monitored by DLS for rNG-DFO incubated with 100 μM H_2O_2 at 0 h (black line), 12 h (red line) and 24 h (blue line). **(C)** Representative UV-Vis absorption spectrum of DFO, rNG and rNG-DFO in the absence and presence of iron(III) reveal that only DFO and rNG-DFO display the characteristic absorbance peak at 430 nm for the DFO:iron(III) complex.

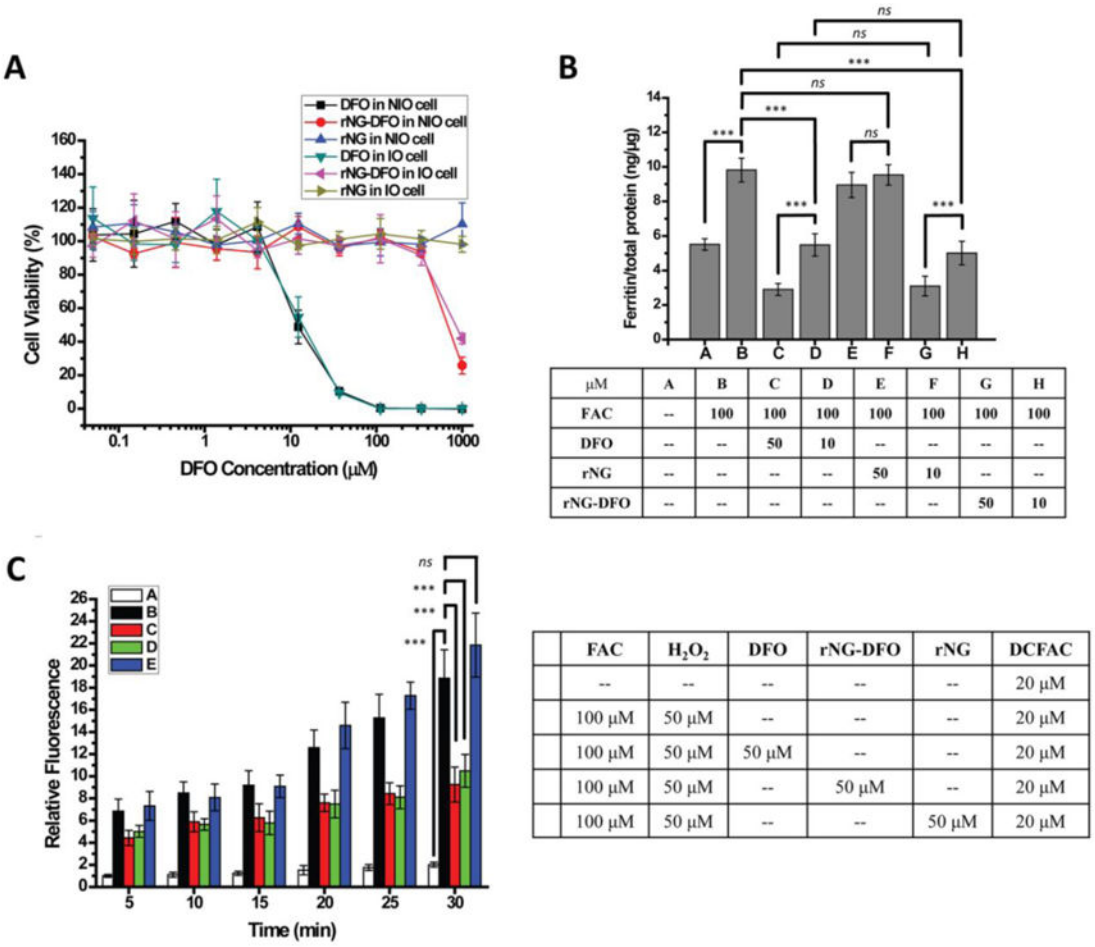

μM	A	B	C	D	E	F	G	H
FAC	--	100	100	100	100	100	100	100
DFO	--	--	50	10	--	--	--	--
rNG	--	--	--	--	50	10	--	--
rNG-DFO	--	--	--	--	--	--	50	10

	FAC	H_2O_2	DFO	rNG-DFO	rNG	DCFAC
	--	--	--	--	--	20 μM
	100 μM	50 μM	--	--	--	20 μM
	100 μM	50 μM	50 μM	--	--	20 μM
	100 μM	50 μM	--	50 μM	--	20 μM
	100 μM	50 μM	--	--	50 μM	20 μM

Fig. 2.

(A) Cytotoxicity of free DFO, rNG and rNG-DFO in NIO and IO macrophage cells after 48 h incubation; a representative set of data is shown where each data point is presented as the mean ± SD ($n = 3$). **(B)** Ferritin reduction ELISA assay to monitor iron chelation efficacy. NIO cells were only treated with DMEM complete medium over the period of the study (**bar A**); cells were IO by 24 h incubation with 100 μM FAC and left untreated (**bar B**); IO cells were treated for 48 h with either 50 μM DFO (**bar C**) or 10 μM DFO (**bar D**), equivalent rNG (**bar E** and **bar F**) based on w/v of rNG-DFO, and 50 μM rNG-DFO (**bar G**) or 10 μM (**bar F**) rNG-DFO to equivalent DFO. Results are normalized to total protein (ng/μg) and presented as mean ± SD (n = 3). "*ns*" means the difference was not significant. *** $p < 0.001$. **(C)** Time dependent iron-mediated oxidative stress levels *in vitro* after incubating IO cells with DFO, rNG, and rNG-DFO. The ROS-sensitive fluorescent probe DCFDA was used as an indicator of ROS levels in cells.

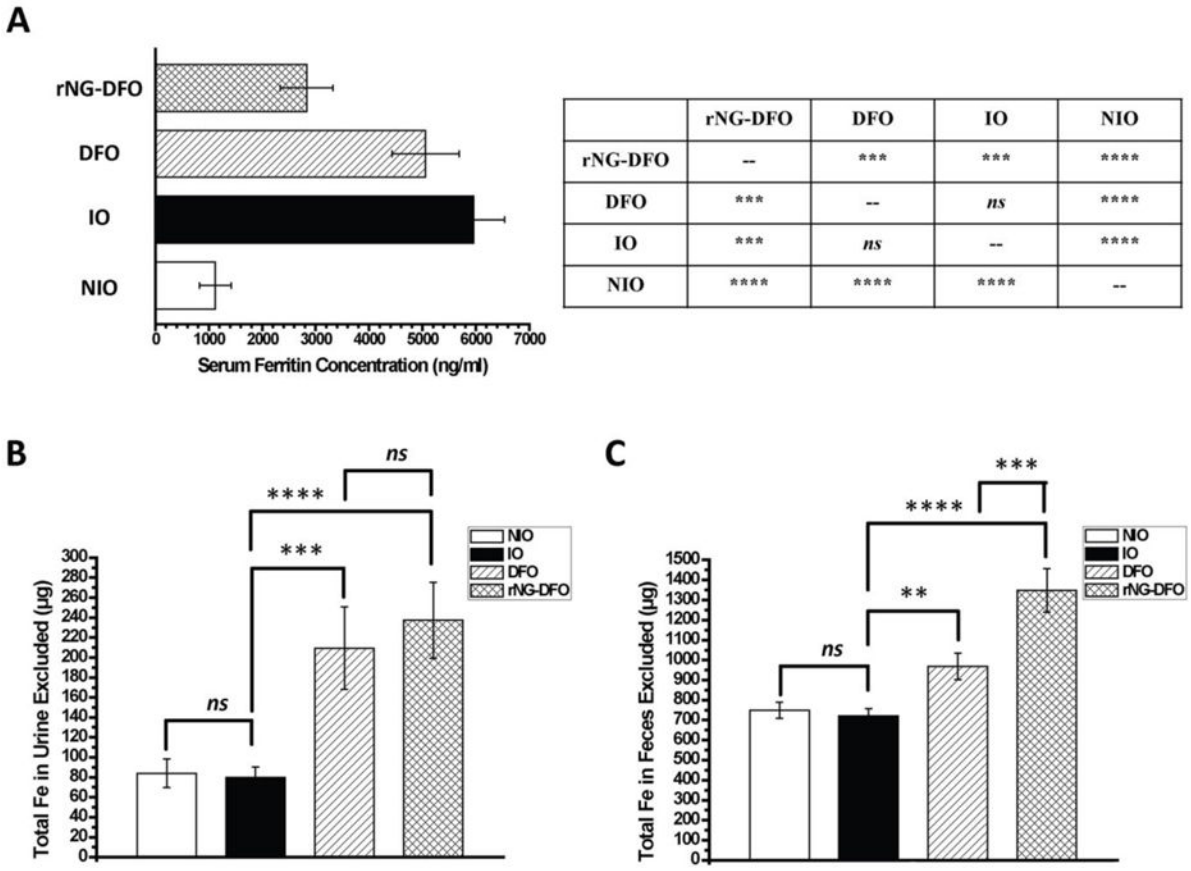

	rNG-DFO	DFO	IO	NIO
rNG-DFO	--	***	***	****
DFO	***	--	*ns*	****
IO	***	*ns*	--	****
NIO	****	****	****	--

Fig. 3.

(A) Final serum ferritin levels in IO mice was measured via a colorimetric mouse ferritin ELISA assay. Statistical significance between the different groups is summarized in the Table next to the bar graph, where results are presented as mean ± SD ($n = 3$), "*ns*" means the difference was not significant, *** $p < 0.001$, and **** $p < 0.0001$. Total iron elimination trends in urine **(B)** and feces **(C)** of IO mice; results are presented as mean ± SD ($n = 3$). "*ns*" means the difference was not significant, ** $p < 0.01$, *** $p < 0.001$, **** $p < 0.0001$.

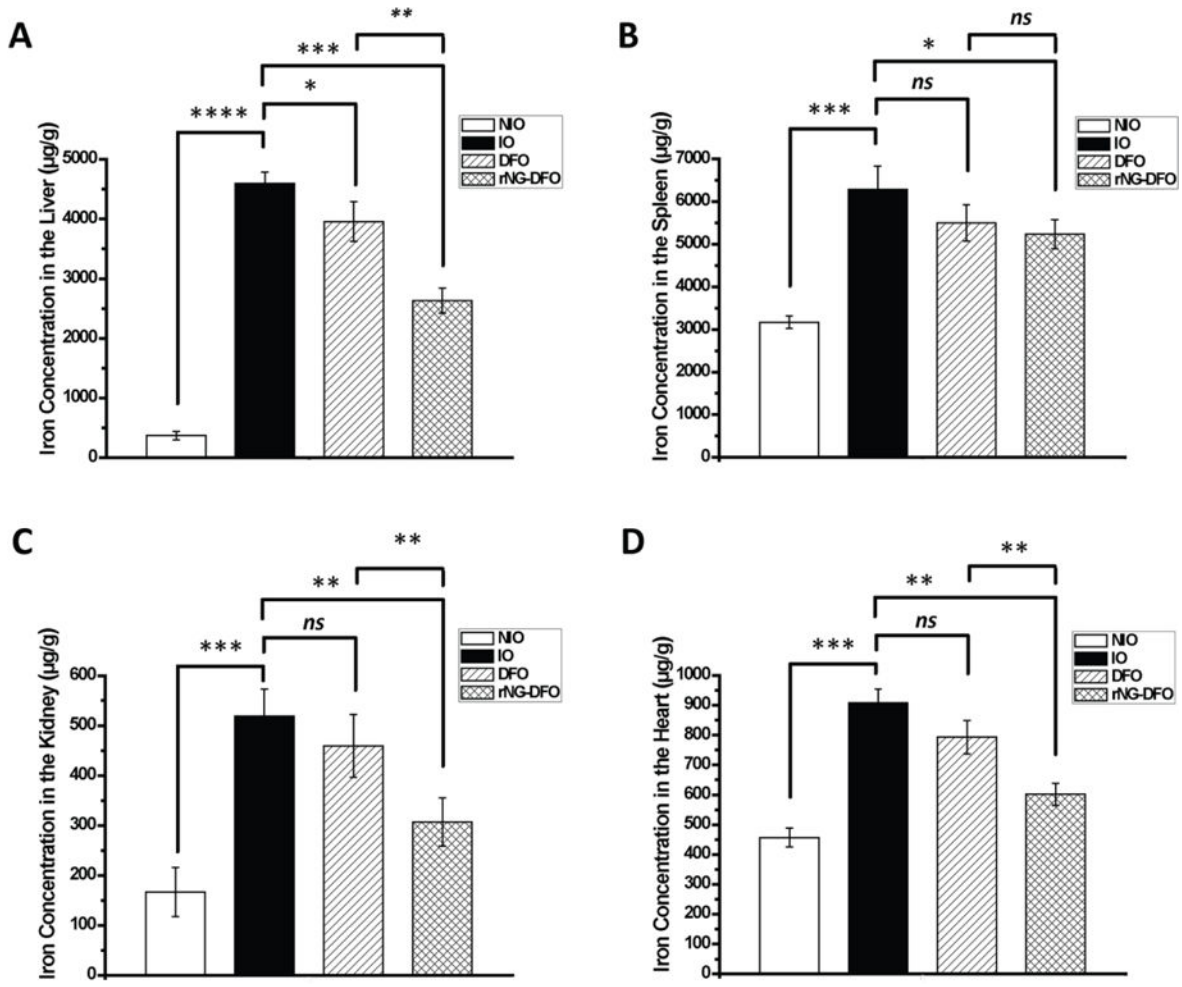

Fig. 4.

Total iron content in **(A)** liver, **(B)** spleen, **(C)** kidney and **(D)** heart as measured by AAS. Results are presented as mean ± SD ($n = 3$). "*ns*" means the difference was not significant, * $p < 0.05$, ** $p < 0.01$, *** $p < 0.001$, **** $p < 0.0001$.

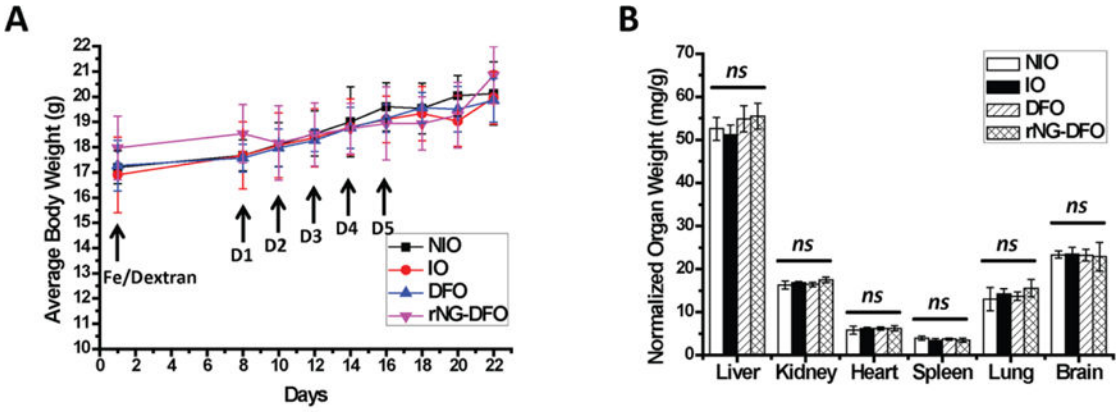

Fig. 5.

Female Balb/C mice were IO by single tail vein injection of Fe/Dextran (150 mg/kg of Fe) on Day 1; treatment with 150 mg/kg of DFO or equivalent rNG-DFO began on Day 8 and was repeated every other day for a total of 5 doses; NIO and untreated IO mice were injected with saline; mice were necropsied 7 days after the last dose. (**A**) BW of mice receiving rNG-DFO and DFO treatments remained within the normal range of ±15% throughout the duration of the study. (**B**) There were no acute signs of toxicity based on normalized organ weights with respect to animal body weight (mg/g). Results are presented as mean ± SD (n = 3). "*ns*" means the difference was not significant.

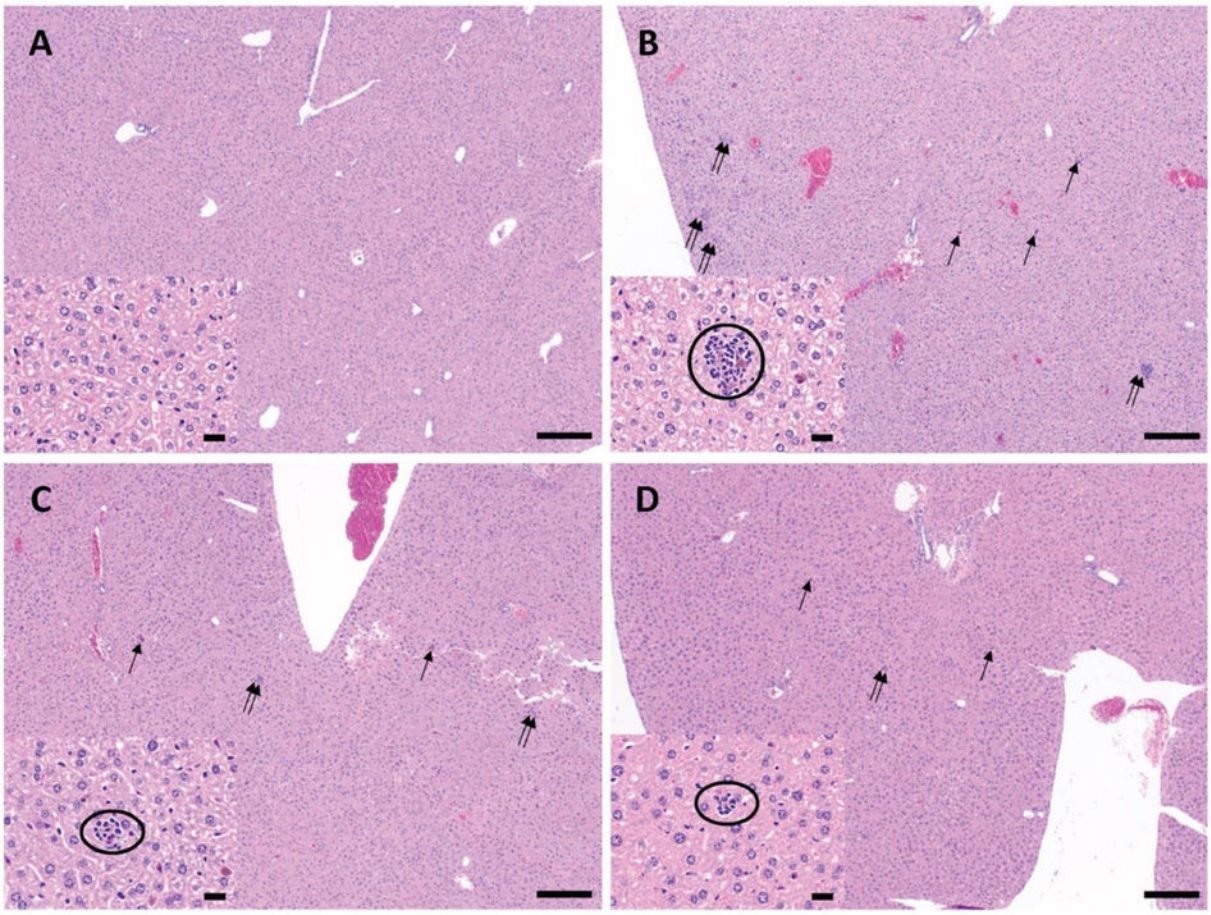

Fig. 6.

Representative photomicrograph of liver sections stained with H&E from the various treatment groups: (**A**) NIO mouse, (**B**) IO mouse without treatment, (**C**) IO mouse with DFO treatment and (**D**) rNG-DFO treatment; double arrows and single arrows are used to show the hypercellularity and iron-containing cells respectively (40× original magnification, scale bar equals 200 μm). Within each panel, the insets show a higher magnification of a selected area where inflammatory cells around a hemosiderin-laden Kupffer cells and minimal cellular debris are circled (400× original magnification, scale bar equals 20 μm).

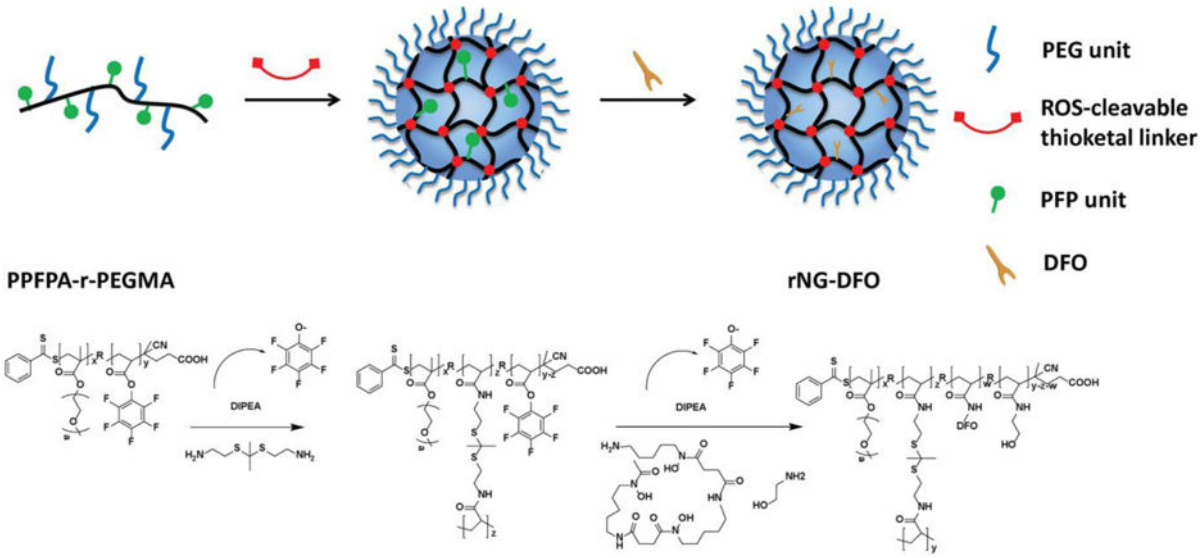

Scheme 1.
Schematic representation for preparing rNG-DFO.

Table 1

Summary comparing histological lesions in major organs after H&E staining, as assessed by a board certified pathologist.

	Liver	Spleen	Heart	Kidney	Lung	Brain
NIO	0 [a)]	0	0	0	0	0
IO	++	0	0	0	0	0
DFO	++	0	0	0	0	0
rNG-DFO	+	0	0	0	0	0

[a)] Focal inflammatory focus around hemosiderin-laden cells: +; Multifocal inflammatory sites around hemosiderin-laden cells: ++; Numerous inflammatory foci around hemosiderin-laden cells: +++; Large number of inflammatory foci around hemosiderin-laden cells: ++++.